Supporting Information

for

Syntheses, Structures and Properties of Ruthenium Complexes of Tridentate Ligands: Isolation and Characterization of a Rare Example of Ruthenium Nitrosyl Complex Containing $\{RuNO\}^5$ Moiety

Kaushik Ghosh*, Rajan Kumar, Sushil Kumar and Jay Singh Meena

Department of Chemistry, Indian Institute of Technology Roorkee,

Roorkee-247667 Uttarakhand INDIA.

E-mail: ghoshfcy@iitr.ernet.in

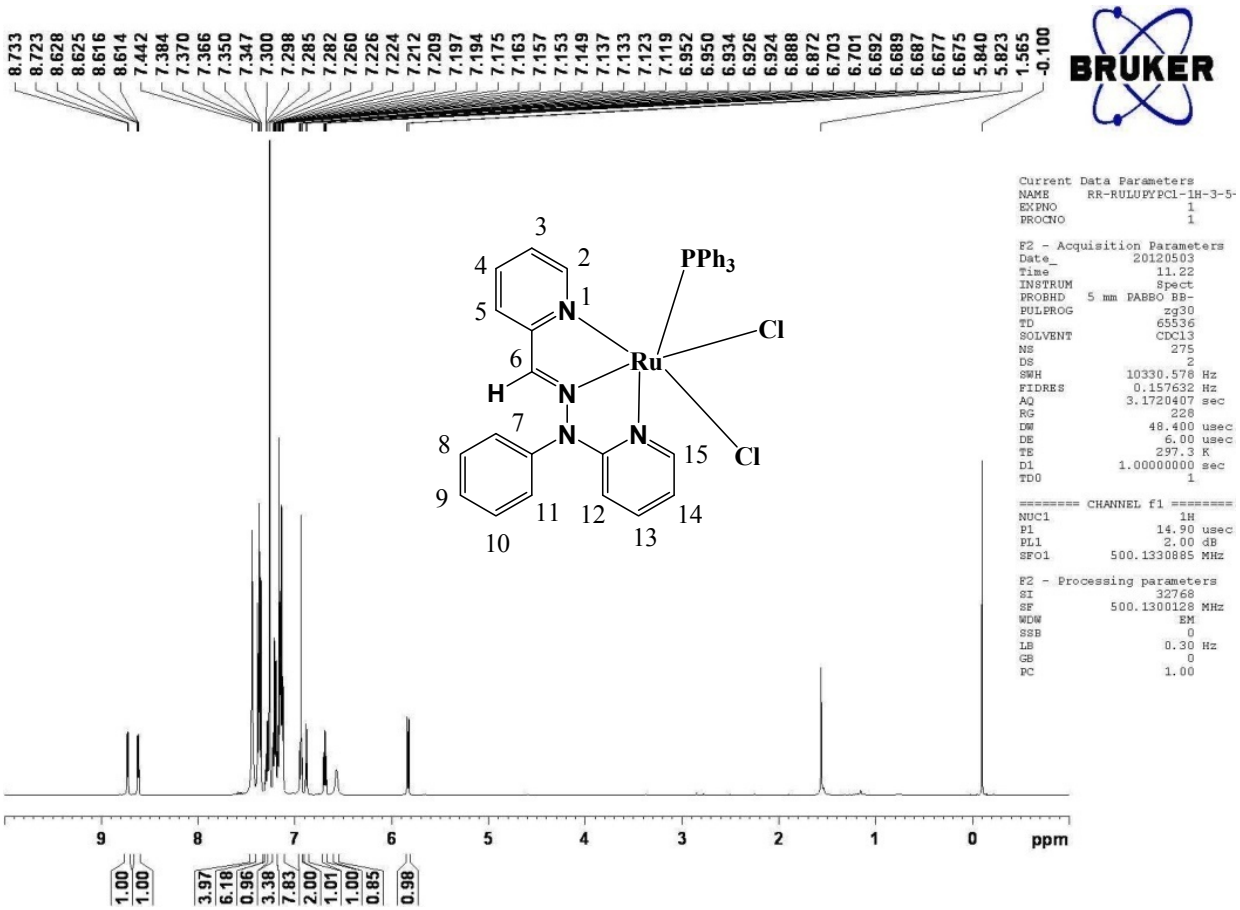

Fig. S1 ^{1}H NMR spectrum of complex **2** in $CDCl_3$ at room temperature.

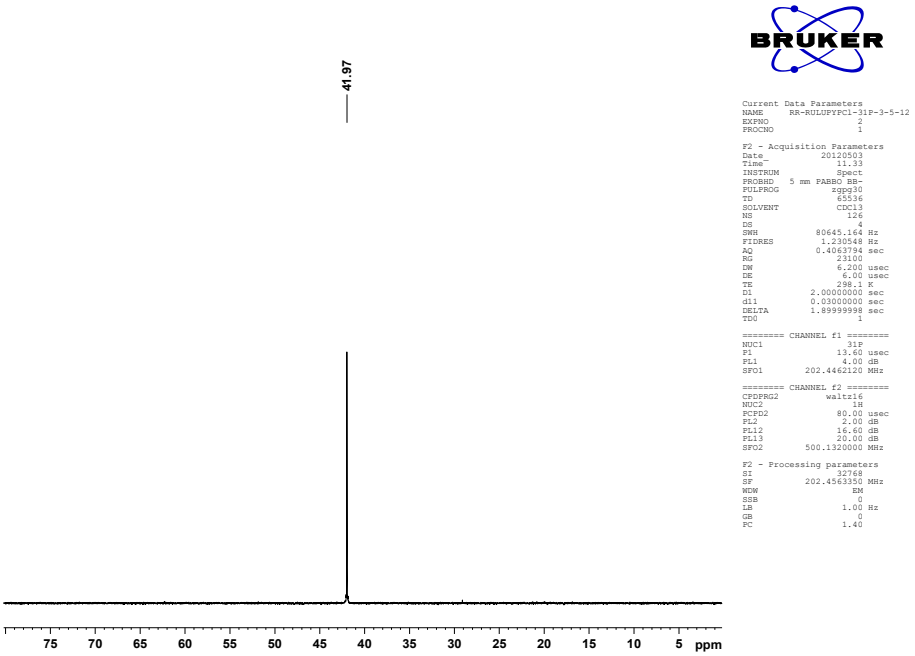

Fig. S2 ^{31}P NMR spectrum of complex **2** in $CDCl_3$ at room temperature.

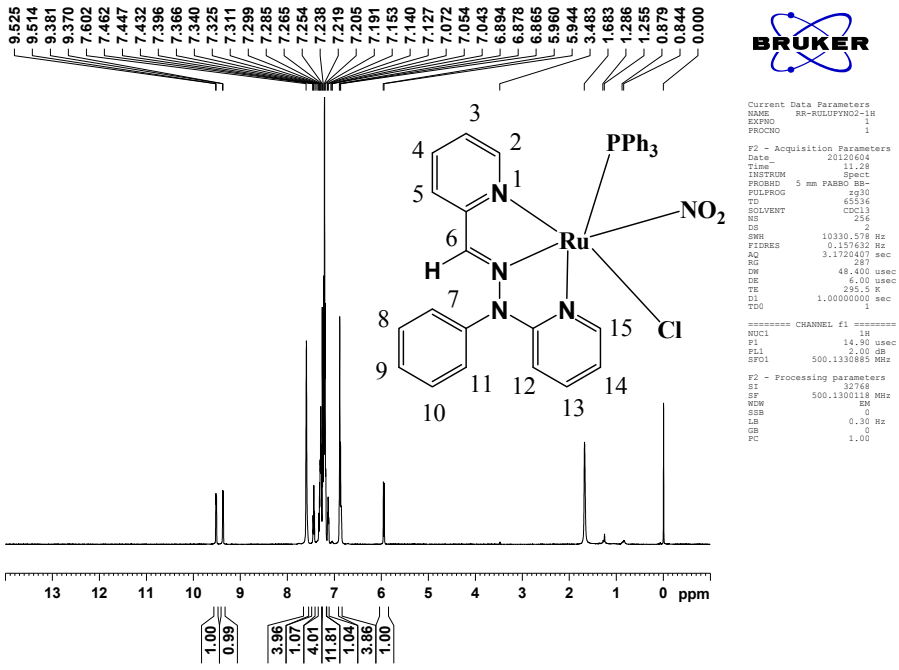

Fig. S3 ^{1}H NMR spectrum of complex **3** in $CDCl_3$ at room temperature.

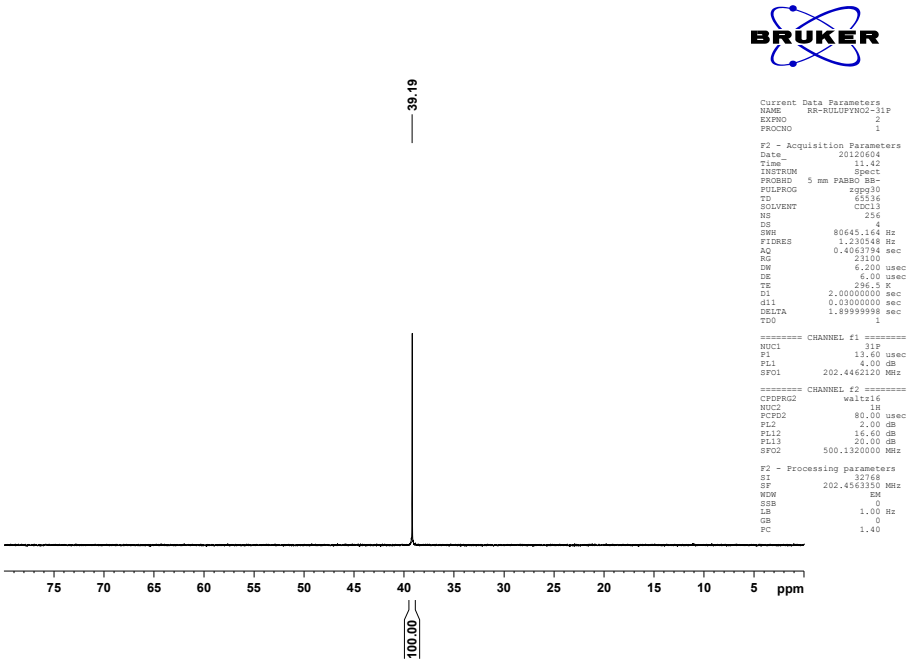

Fig. S4 ^{31}P NMR spectrum of complex **3** in $CDCl_3$ at room temperature.

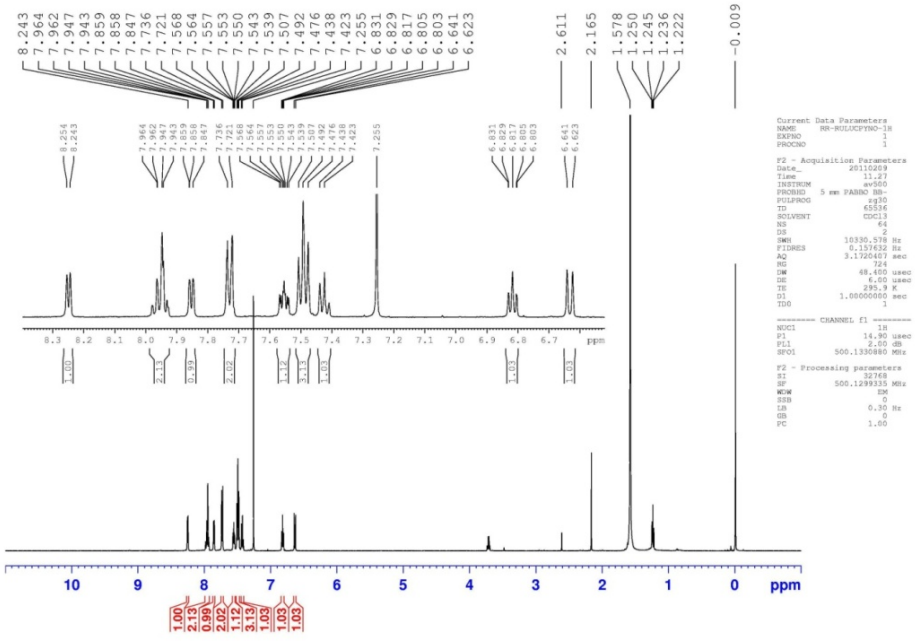

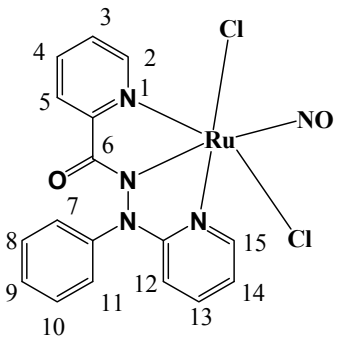

Fig. S5 ^{1}H NMR spectrum of complex **1** in $CDCl_3$ at room temperature.

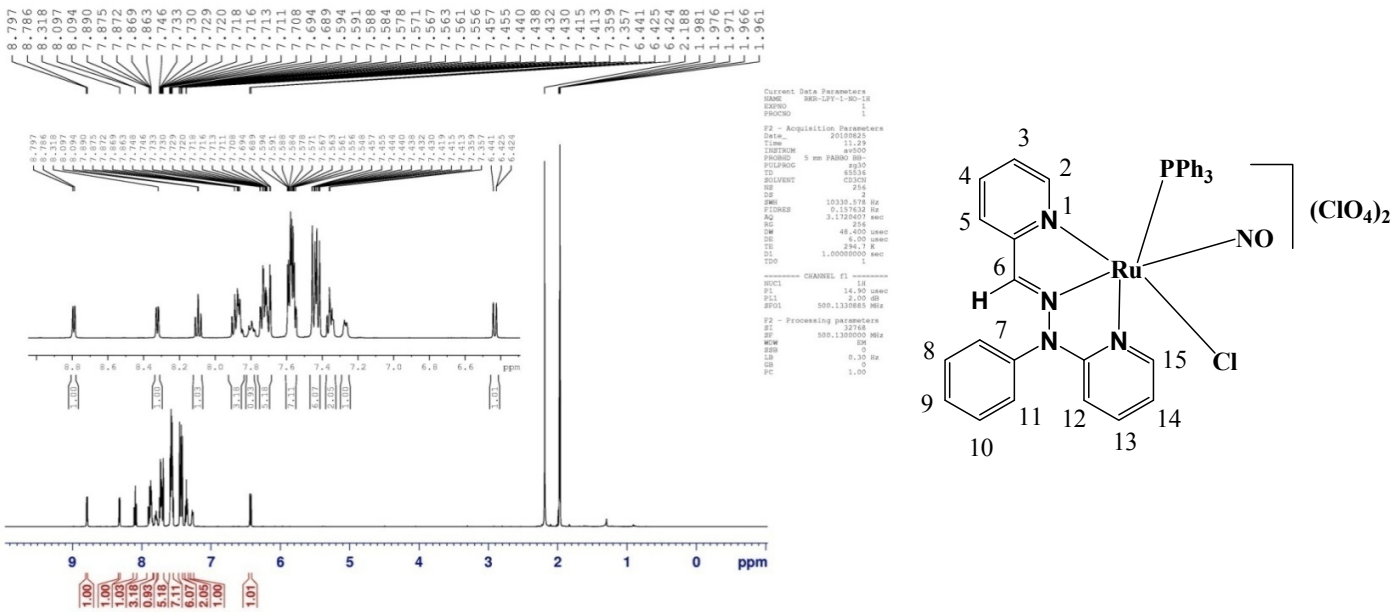

Fig. S6 ^{1}H NMR spectrum of complex **4** in CD_3CN at room temperature.

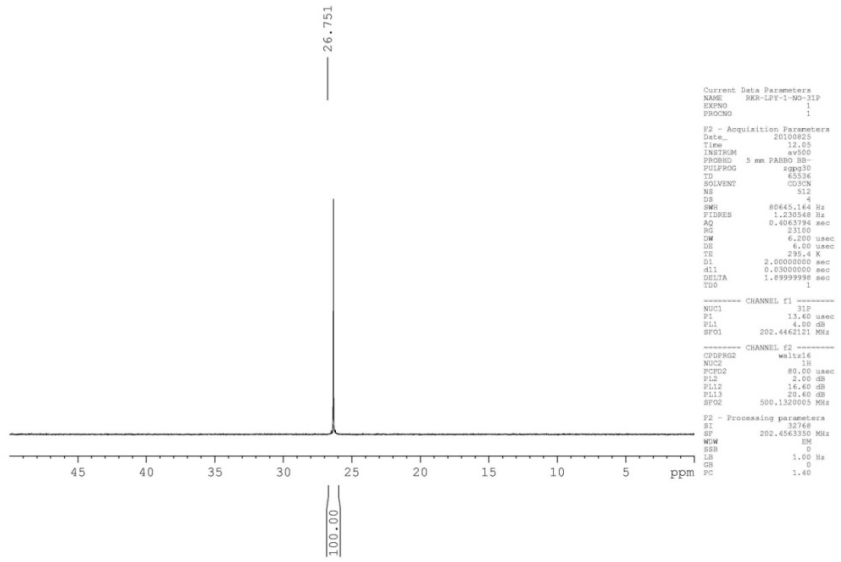

Fig. S7 ^{31}P NMR spectrum of complex **4** in $CDCl_3$ at room temperature.

Table S1 ^{1}H NMR Spectral Data [δ, ppm (*J*, Hz)] of Complexs **1**, **2**, **3**, **4**.

Compd	2–H	11–H	7–H	15–H	6–H	Other protons
1	8.25	6.67	6.84	7.84	–	7.93–7.4 (ligand–H)
2	8.73	5.84	6.57	8.62	7.34	7.44–6.92 (PPh_3, 15H and ligand–H)
3	9.52	5.95	6.86	9.37	7.45	7.34–7.12 (PPh_3, 15H and ligand–H)
4	8.79	6.43	7.35	8.31	7.63	7.89–7.48 (PPh_3, 15H and ligand–H)

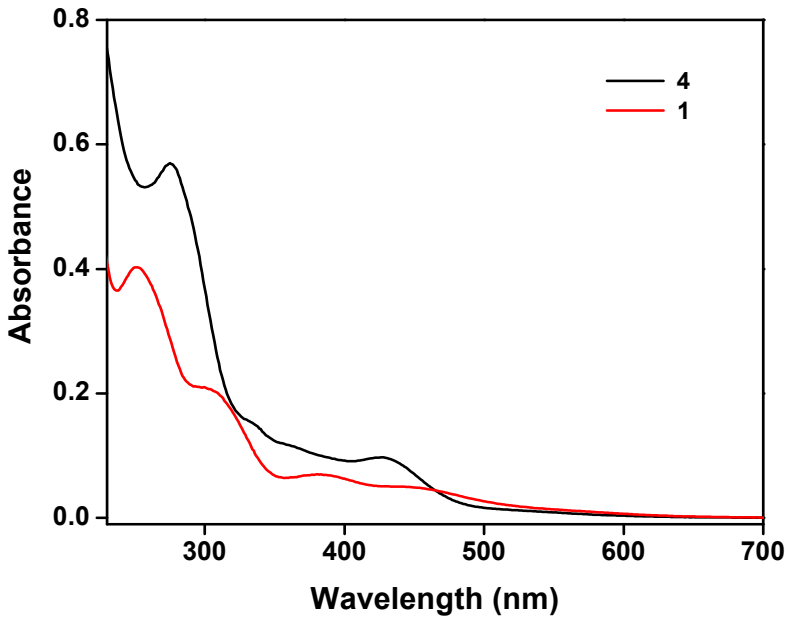

Fig. S8 Electronic absorption spectra of **1** (red line) and **4** (black line) in acetonitrile solutions.

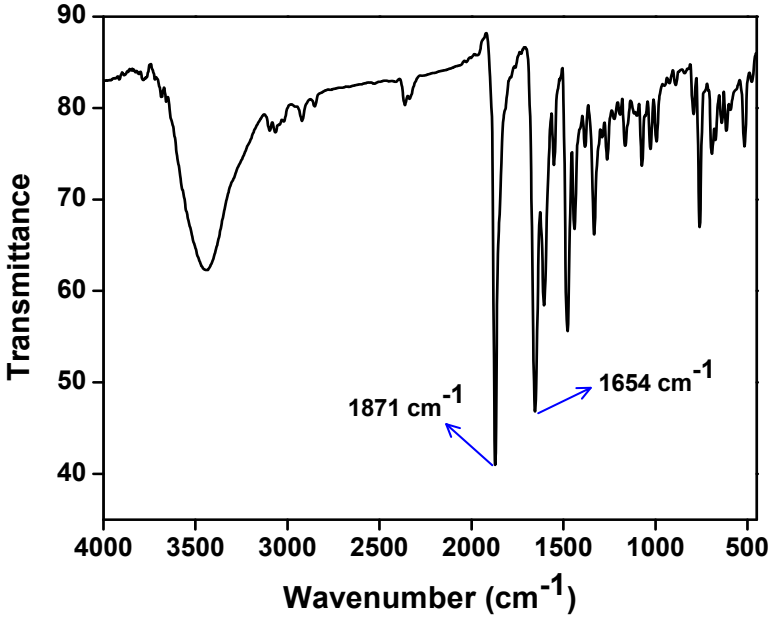

Fig. S9 Infrared spectrum of complex **1**. IR (KBr disk, cm^{-1}): 1871 (ν_{NO}) and 1654 (ν_{CONH}) cm^{-1}.

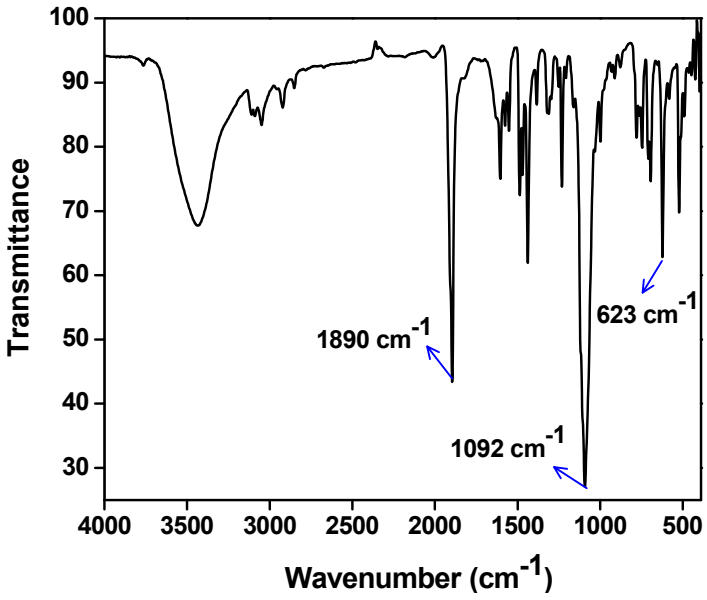

Fig. S10 Infrared spectrum of complex **4**. IR (KBr disk, cm^{-1}): 1890 (ν_{NO}), 1092, 623 (ν_{ClO4}), 746, 694, 522 (ν_{PPh3}) cm^{-1}.

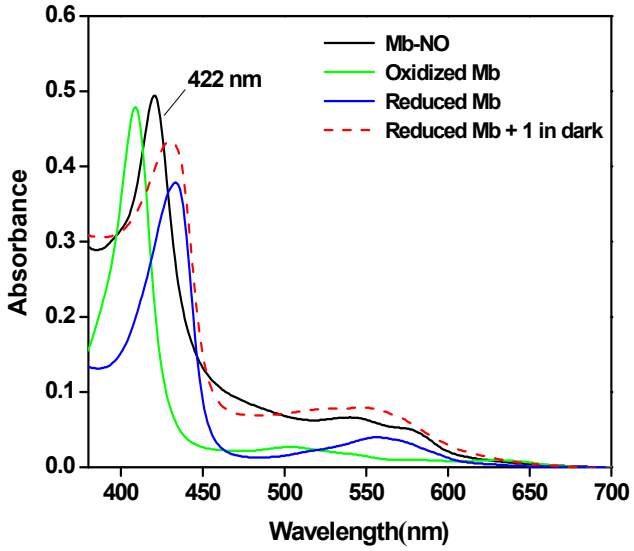

Fig. S11 Electronic spectra of conversion of reduced myoglobin to Mb─NO adduct upon reaction with **1** in buffer solution (50 mM phosphate buffer, pH 6.8) under exposure of UV light. Green line, Met Mb (intense band at 409 nm); blue line, reduced Mb (near 433 nm, with excess of sodium dithionite); red dotted line, reduced Mb + solution of **1** (~ 4.5 x 10^{-5} M) in dark; black line, Mb─NO adduct for **1** at 422 nm when same solutions were exposed to UV light for 2-3 minutes.

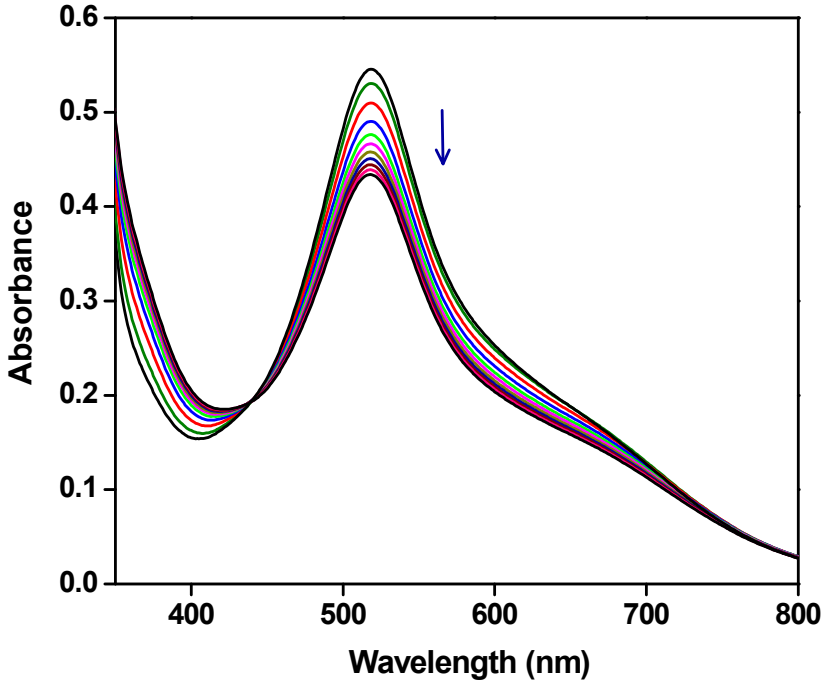

Fig. S12 Reaction of photoreleased NO derived from complex **1** with DPPH radical (~ 10^{-5} M) in acetonitrile solution.

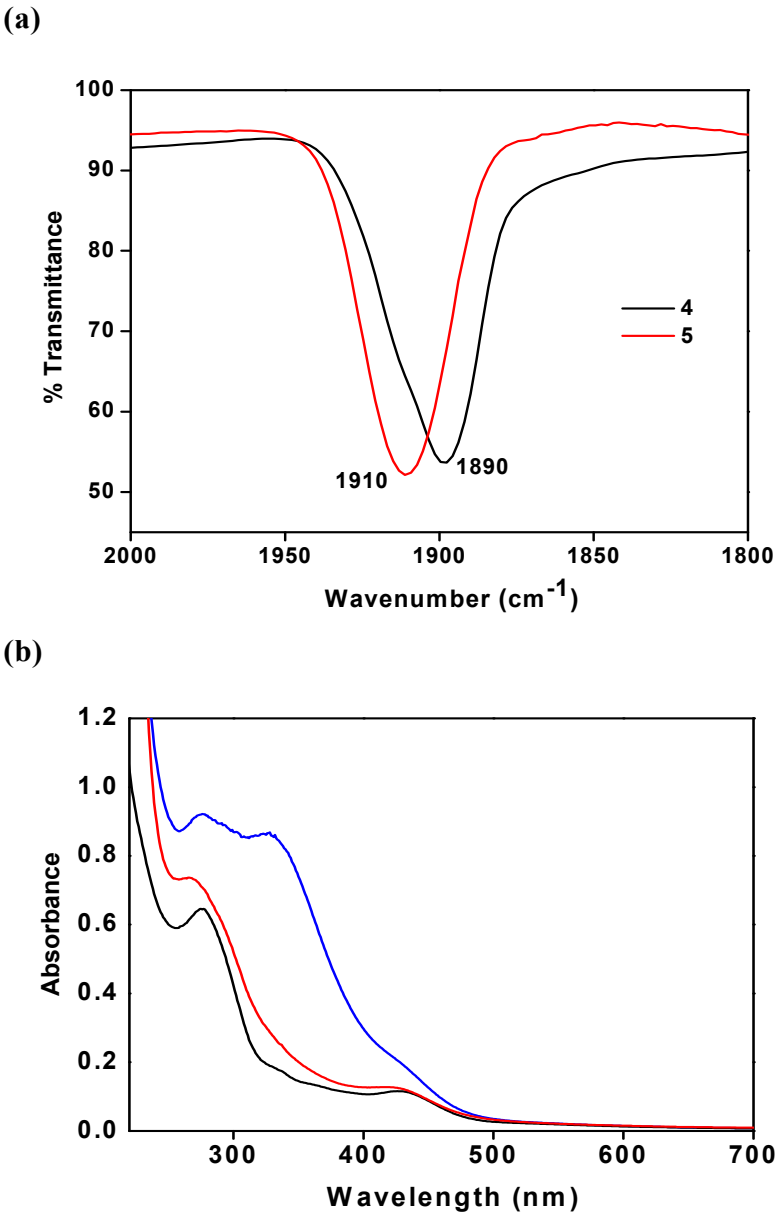

Fig. S13 (a) Infrared and (b) UV-Vis spectra (black line, complex **4**; blue line, **4** (1 mM) + CAN (8 mM); red line, **4** (1 mM) + CAN (8 mM) + sodium dithionite (2 mM)) showing the conversion of $\{RuNO\}^6$ to $\{RuNO\}^5$ species when complex **4** was treated with ceric ammonium nitrate in acetonitrile solution.

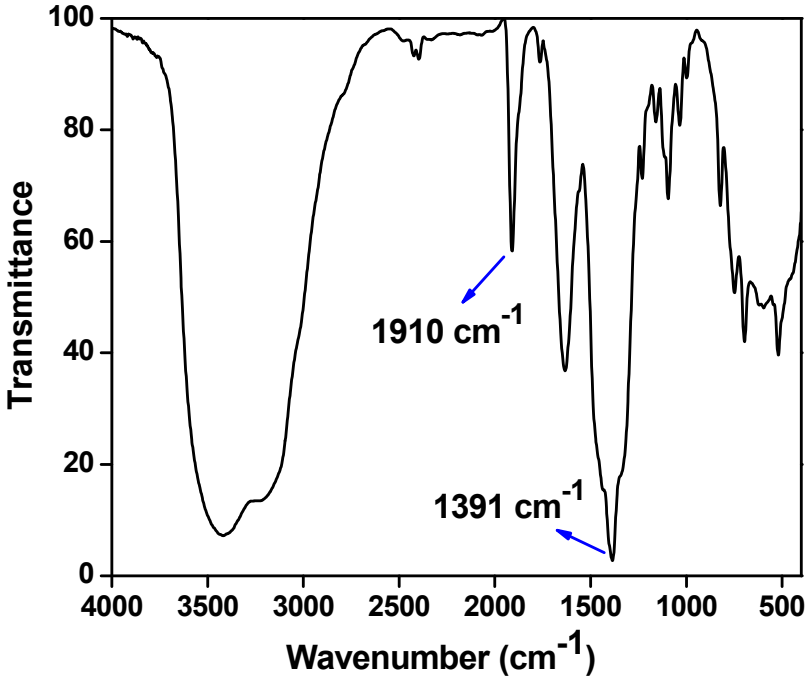

Fig. S14 Infrared spectrum of complex **5**. IR (KBr disk, cm^{-1}): 1910 (ν_{NO}), 1391 (ν_{NO3}), 1085, 750, 695, 518 (ν_{PPh3}) cm^{-1}.

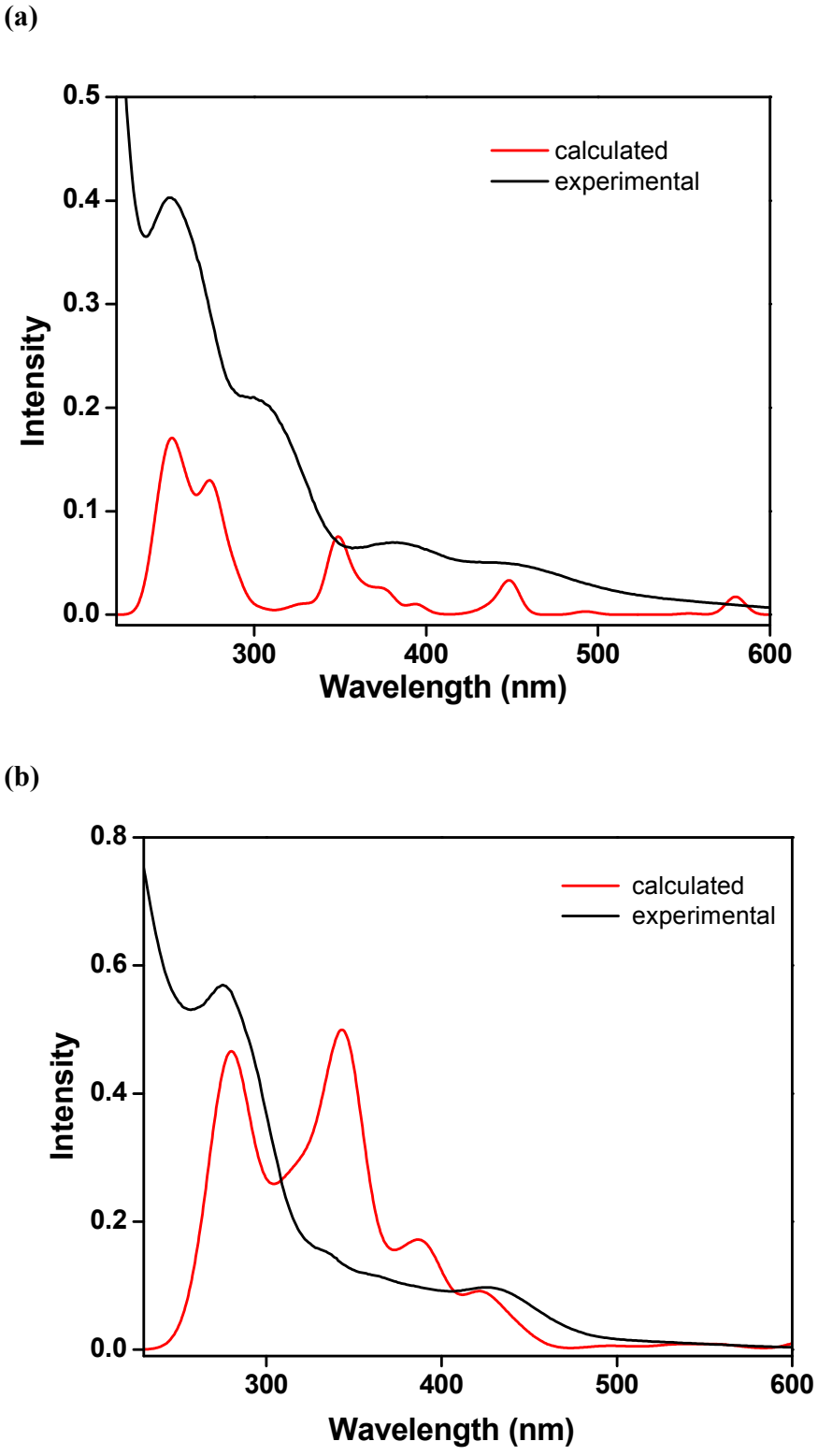

Fig. S15 Experimental and TDDFT calculated absorption spectra of (a) complex **1** and (b) complex **4**.

Table S2 Selected bond distances (Å) and bond angles (°) for nitrosyl complexes **1** and **4** along with the optimized DFT bond parameters for comparison.

Bond lengths (Å)			**Bond angles (deg.)**		
			Complex **1**		
	X-ray	**DFT**		**X-ray**	**DFT**
Ru(1)−Cl(1)	2.3678(8)	2.471	N(1)−Ru(1)−N(4)	157.61(8)	156.81
Ru(1)−Cl(2)	2.3882(8)	2.499	N(2)−Ru(1)−N(5)	173.51(10)	174.22
Ru(1)−N(2)	1.977(2)	1.993	Cl(1)Ru(1)−Cl(2)	175.55(3)	176.14
Ru(1)−N(1)	2.074(2)	2.083	N(1)−Ru(1)−N(2)	79.12(9)	78.16
Ru(1)−N(4)	2.052(2)	2.098	N(4)−Ru(1)−N(2)	78.59(9)	78.91
Ru(1)−N(5)	1.761(2)	1.782	N(4)−Ru(1)− Cl (1)	88.88(7)	87.76
N(5)−O(2)	1.147(3)	1.197	N(4)−Ru(1)− Cl (2)	90.14(7)	92.05
			O(2)−N(5)−Ru(1)	169.4(2)	171.89
			Complex **4**		
Ru(1)−Cl(1)	2.3858(12)	2.473	N(3)−Ru(1)−N(2)	77.71(15)	77.70
Ru(1)−P(1)	2.4057(13)	2.581	N(1)−Ru(1)−N(4)	96.44(16)	103.03
Ru(1)−N(4)	2.082(3)	2.118	P(1)−Ru(1)−Cl(1)	173.71(5)	175.35
Ru(1)−N(3)	2.002(4)	2.051	N(4)−Ru(1)−N(3)	78.17(15)	78.13
Ru(1)−N(2)	2.077(3)	2.100	N(4)−Ru(1)−N(2)	155.39(14)	155.52
Ru(1)−N(1)	1.731(4)	1.776	N(2)−Ru(1)−P(1)	92.53(9)	93.94
N(1)−O(1)	1.142(4)	1.184	N(1)−Ru(1)−P(1)	89.88(12)	94.95
			O(1)−N(1)−Ru(1)	173.7(4)	172.31

Table S3 Calculated HOMO compositions (in %) expressed in terms of individual fragments.

Complex	**Ru**	**Cl**	**NO**	**Other**
$[Ru(L^1)(NO)Cl_2]$ (**1**)	2	6	8	83
$[Ru(L^2)(PPh_3)(NO)Cl]^{2+}$ (**4**)	5	6	0	89
$[Ru(L^2)(PPh_3)(NO)Cl]^{3+}$ (**5**)	8	7	1	84

Table S4 Calculated TD-DFT excitation energies (in eV), oscillator strengths (*f*), and nature of transitions in the complexes **1** and **4**.

.

Composition	E (eV)	Oscillator strength (*f*)	λ_{theo} (nm)	λ_{exp} (nm)
Complex 1				
HOMO → LUMO+2 (88%) HOMO–1 → LUMO+3 (6%)	2.76	0.0309	448.98	442
HOMO→ LUMO+5 (49%) HOMO–12 → LUMO+1 (17%) HOMO–1 → LUMO+6 (4%) HOMO–2 → LUMO+2 (3%) HOMO–10 → LUMO+1 (3%) HOMO–3 → LUMO+2 (3%)	3.56	0.0366	348.20	383
HOMO–12 → LUMO (13%) HOMO–3 → LUMO+4 (13%) HOMO–13 → LUMO+1 (11%) HOMO–14 → LUMO+1 (10%) HOMO–10 → LUMO+1 (7%) HOMO–9 → LUMO+1 (5%) HOMO–3 → LUMO+5 (4%) HOMO–13 → LUMO (4%) HOMO–14 → LUMO (3%)	4.52	0.0609	274.11	274
HOMO–10 → LUMO+2 (53%) HOMO–7 → LUMO+4 (9%) HOMO–11 → LUMO+2 (7%) HOMO–10 → LUMO+3 (3%) HOMO–7 → LUMO+5 (3%) HOMO–1 → LUMO+7 (2%) HOMO–5 → LUMO+6 (2%)	4.91	0.0726	252.67	250

Complex 4				
HOMO → LUMO+2 (63%) HOMO–2 → LUMO+2 (3%) HOMO–5 → LUMO+2 (3%) HOMO–4 → LUMO+2 (5%) HOMO–6 → LUMO+2 (7%) HOMO–11 → LUMO (15%)	2.94	0.0355	420.98	425
HOMO–1 → LUMO+6 (4%) HOMO–1 → LUMO+5 (3%) HOMO–9 → LUMO+4 (45%) HOMO → LUMO+6 (8%) HOMO–10 → LUMO+4 (24%) HOMO–6 → LUMO+5 (3%) HOMO–12 → LUMO+2 (2%) HOMO–8 → LUMO+4 (2%)	4.42	0.0429	280.62	275

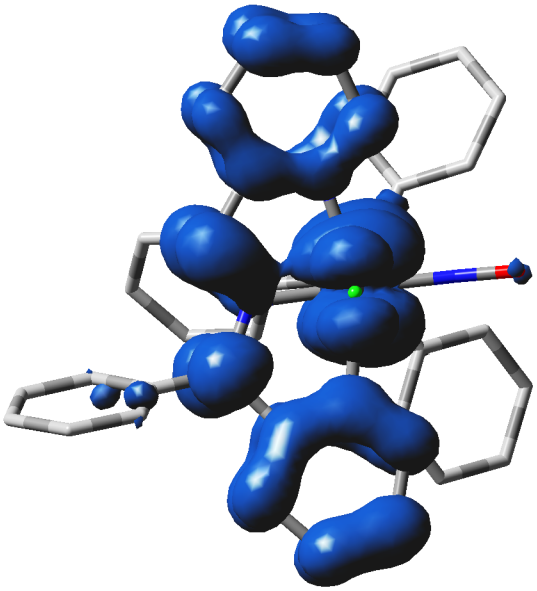

Fig S16 Spin density distribution in complex **5**.

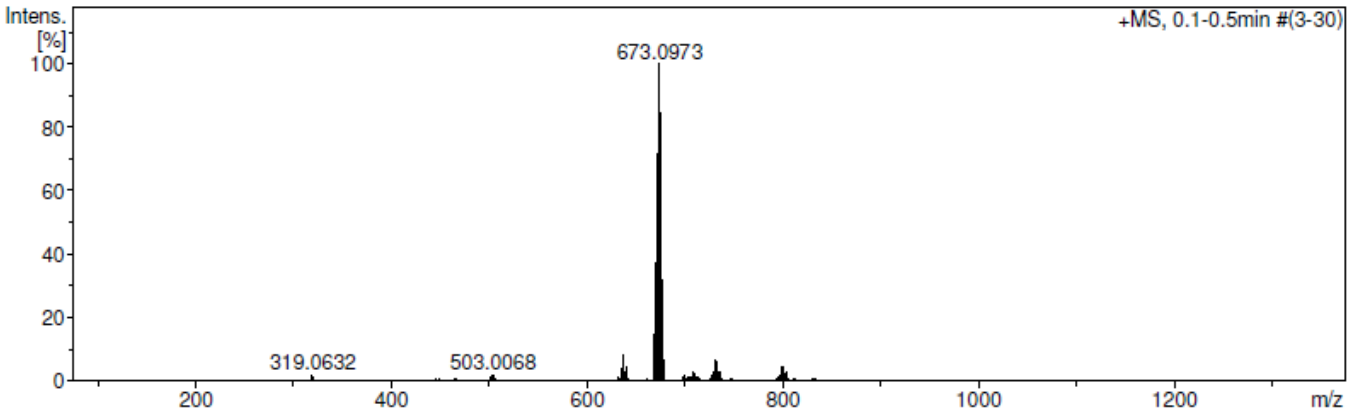

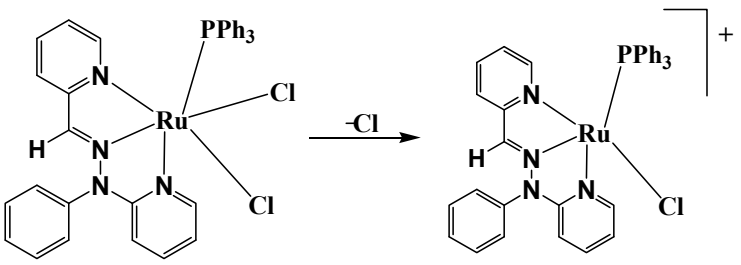

m/z = 708.06 $(M)^+$ *m/z* = 673.09 $(M\text{-}Cl)^+$

Fig. S17 ESI-MS spectrum of complex **2** along with fragmentation pattern.

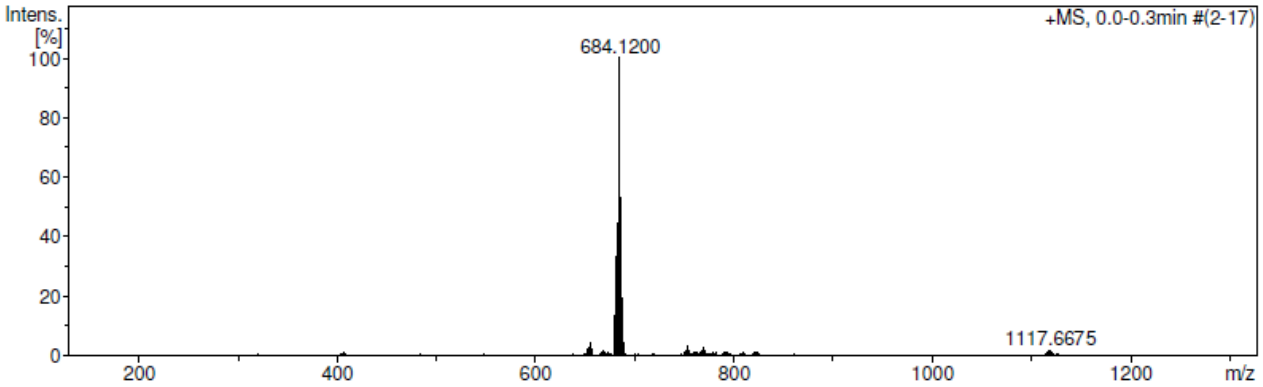

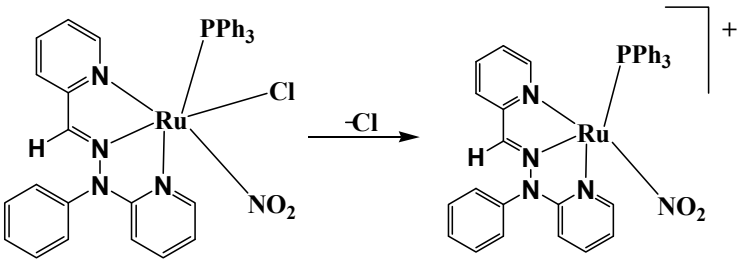

m/z = 719.08 $(M)^+$ *m/z* = 684.11 $(M\text{-}Cl)^+$

Fig. S18 ESI-MS spectrum of complex **3** along with fragmentation pattern.

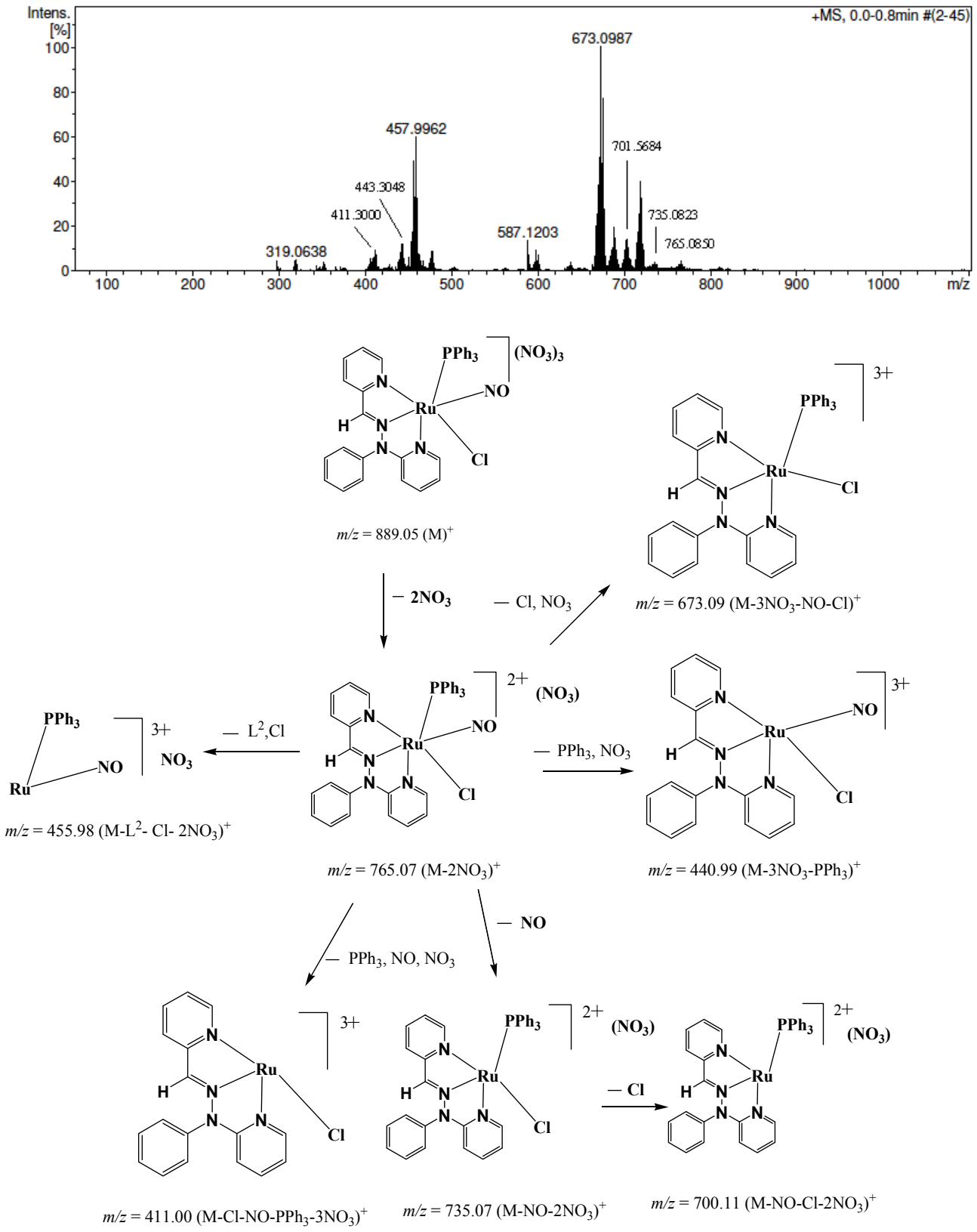

Fig. S19 ESI-MS spectrum of complex **5** along with fragmentation pattern.